# A Model and Application of Vibratory Surface Grinding

**Abstract:** This paper presents a model of surface grinding with superimposed oscillation of the workpiece. The parameters of the model were derived experimental and the equations of motions of the system were solved using MatLab. The results obtained showed a significant decrease in the amplitude of the relative vibration between the wheel and workpiece when the oscillation was superimposed onto the feed motion of the workpiece. A range of experimental work was undertaken and the results showed that the vibratory process had a better performance in absolute terms with reference to conventional grinding. Low forces along with longer tool life was recorded with the added vibration. A notion of "dynamic relief" was introduced to express the efficiency of the vibratory process.

**Key-words**: vibratory surface grinding, machine tool mathematical model

Nomenclature

| **Parameter** | **Comment** |
|---|---|
| $m_1$, kg | Mass of the grinder table |
| $m_2$, kg | Mass of the vibratory table and the workpiece |
| $m_w$, kg | Mass of the spindle |
| $m_3$, kg | Mass of the wheel |
| $m_4$, kg | Mass of the pulley |
| $m_z$ = 6 kg | Total mass of the spindle unit (spindle $m_w$ + wheel $m_3$ + pulley $m_4$) |
| $B_{2y}$, kgm$^2$ | Moment of inertia of oscillating table ($m_2$) with workpiece |
| $B_z$ , kgm$^2$ | Principal moment of inertia of the spindle unit(spindle $m_w$ + wheel $m_3$ + pulley $m_4$) |
| $J$, kgm$^2$ | Moment of inertia of the spindle with wheel and pulley in $y$ axis |
| $k_1$, N/m | Stiffness of the grinder table drive unit in $x$ direction |
| $c_1$, Ns/m | Damping of the grinder table drive unit in $x$ direction |
| $k_2$, N/m | Stiffness of the blocked vibratory table in $x$ direction |
| $c_2$, Ns/m | Damping of the blocked vibratory table in $x$ direction |
| $k^*_2$, N/m | Stiffness of the unblocked vibratory table in $x$ direction |
| $c^*_2$, Ns/m | Damping of the unblocked vibratory table in $x$ direction |
| $k_3$, N/m | Contact stiffness of the wheel/workpiece |
| $k_{4x}$=$k_{5x,}$ N/m | Stiffness of the spindle bearing unit in $x$ direction |
| $c_{4x}$=$c_{4x,}$ Ns/m | Damping of the spindle bearing unit in $x$ direction |
| $k_{4z}$ = $k_{5z,}$ N/m | Stiffness of the spindle bearing unit in $z$ direction |
| $c_{4z}$ = $c_{5z,}$ Ns/m | Damping of the spindle bearing unit in $z$ direction |
| $k_6$, N/m | Stiffness of the vibratory table in $z$ direction |
| $K$ = 2000, N | Coefficient of proportionality of grinding force, |
| $C_{St1}$ = 8000 | Static cutting edges density at a depth $z=1mm$, [mm$^{-3}$]; |
| $v_0$, = $v_{ft}$ m/min | Constant table feed rate |
| $a_n$, mm | Set depth of cut |
| $d_s$, mm | Grinding wheel diameter (200) |
| $A_0$, μm | Amplitude of wheel eccentric forces - $F_{w1x} = F_{w1z}$ |
| $A_{vib}$, μm | Workpiece vibration amplitude |
| $f_{vib}$, Hz | Workpiece vibration frequency |
| $f$, Hz | Frequency of excitation |

| | |
|---|---|
| $l_1$, $l_2$, $l_3$, $l_4$, $l_5$, m | Geometric dimensions of the physical model, in Fig.6 |
| $A_1$ | Amplitude of the force |
| $A_2$, m | Amplitude of excitation |
| $m_d$ | Unbalanced mass |
| $r$ | Radius of unbalance |
| $t$, $s$ | Time |
| $a_{es}(t)$, mm | Wheel profile |
| $b_D$ = 20, mm | Width of grinding |
| $v_s$ = 30, m/s | Surface velocity of the wheel |
| $aew(t)$, mm | The workpiece profile |
| $v_{w2}(t)$, m/min | Oscillating table speed |
| $vft$, m/min | Table speed, [m/min |
| $\dot{z}_3$ | Speed of the massless point of contact between the grinding wheel and the Workpiece in the normal direction |
| $\dot{x}_3$ | Speed of massless point of contact between the grinding wheel and the Workpiece in the tangent direction |
| $\omega_0$ | Rotational speed of the wheel |
| $\varepsilon$ = 0,8 | Exponent |
| $\gamma$ = 1 | Exponent |
| $\mu$ | Grinding force ratio |
| $\tau_p$ | Workpiece time delay |
| $\tau_s$ | Wheel time delay |
| $\omega_0$ | Angular speed of the grinding wheel |
| $\omega_n$ | Angular speed of precession caused by $F_n$ |
| $\omega t$ | Angular speed of precession caused by $F_t$ |
| $\beta$ | Relief due to vibratory process |

## 1. Introduction

During the design and construction process, as well as in the maintenance of machine tools, special attention must be paid to dynamical processes (vibrations) that affect the Machine Tool-Workpiece (MTW) system. These dynamic phenomena have the great impact on the performance of the machine tools. The quality of the machined surface is a result of the relative motion of the cutting tool and the workpiece, and the accuracy of the machining process is highly dependent on the control or management of the deviation of the real and assumed trajectories of the cutting tool [1], [2].

All vibro-acoustic processes which occur during abrasive processing (grinding) are mutually connected within the dynamic structure of Machine Tool-Workpiece system. Vibrations which occur during the surface grinding process, as illustrated in Fig.1, can be divided into three groups: free, forced and self-excited vibrations [3]. In the case of brittle materials (e.g. ceramics) hybrid methods of abrasive machining [4], [5] are used, consisting of simultaneous application of different forms of energy in order to remove the allowance material. The method of vibratory grinding, in which the kinematics of traditional grinding is combined with additional oscillatory movement of the workpiece at given amplitude and frequency, is one example of a hybrid method of grinding.

The imposed vibrations cause changes in the magnitude of grinding speed which leads to modifications in mechanisms of cheap formation and grinding wheel wear processes. Additionally, the modified movements result in better waviness finish of the surface and reduction of the grinding forces. The latter result is of a great importance since lower grinding forces cause lower thermal deflection of the machined workpiece. This induces less subsurface damage, fewer micro-cracks and less burn of the ground surface.

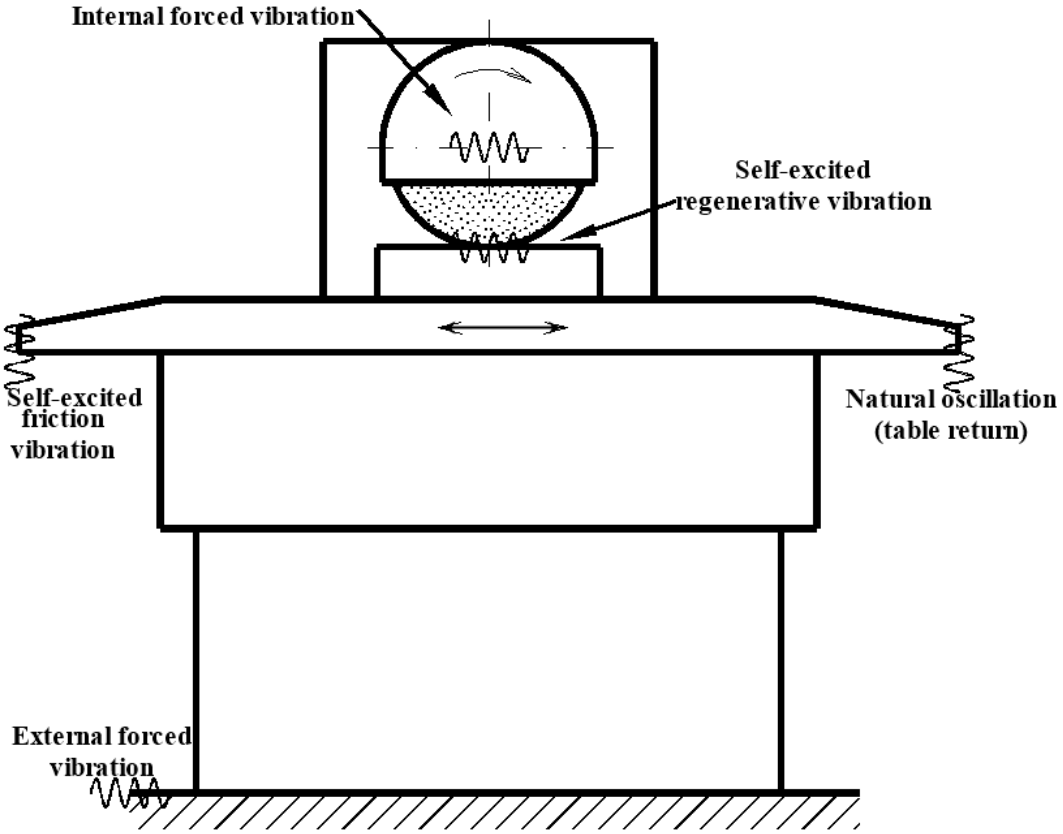


**Fig. 1.** Typical vibrations in a surface grinder

The aim of this paper is to create a robust model of vibratory flat grinding, which includes both process and machine tool responses. The model is needed to predict the dynamic behaviour of a flat grinder subjected to modified kinematics of grinding process, by adding vibration to the workpiece in the direction, which is at the parallel tangent to the wheel (modified table speed).

## 2. The surface grinder

The SPC-20 surface grinder used in this study, shown in Fig. 2, is equipped with slide-rolling wheel spindle bearings, a table with hydraulic drive and slide guideways. In order to adapt the grinder to the needs of vibratory flat grinding process, an additional device was designed which allows inducing controlled vibration of the workpiece during grinding. A sketch of the oscillating table is depicted in Fig.3, and consists of the base 1 on which the rolling guideways 2 were placed.

The workpiece holder 3 moved along the guideways in one direction. The oscillatory movement of the workpiece 4 was induced with the electrodynamic exciter 5. The exciter allowed a maximum amplitude of 50 μm at frequency in the range of 20 Hz ÷ 10 kHz.

The oscillating table was mounted directly on the grinder table in order to induce controlled vibration of the workpiece.

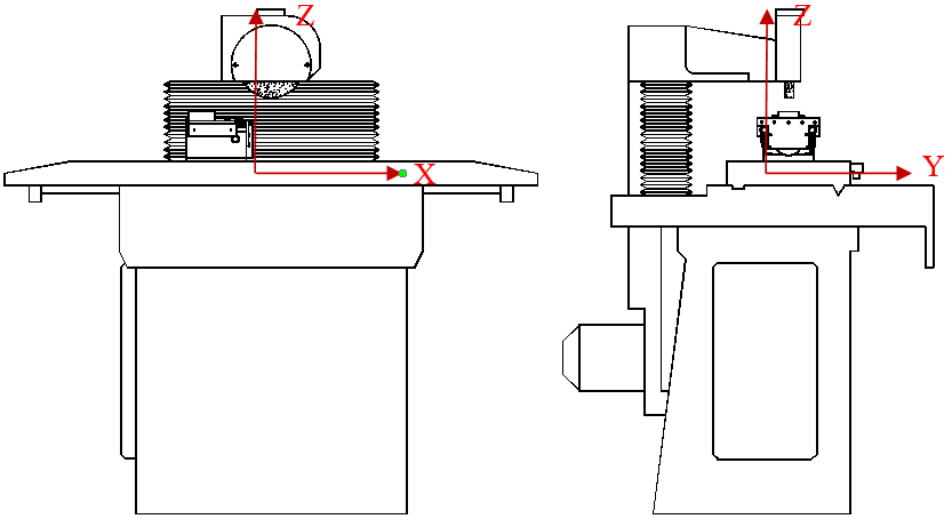


**Fig. 2.** The SPC 20 surface grinder

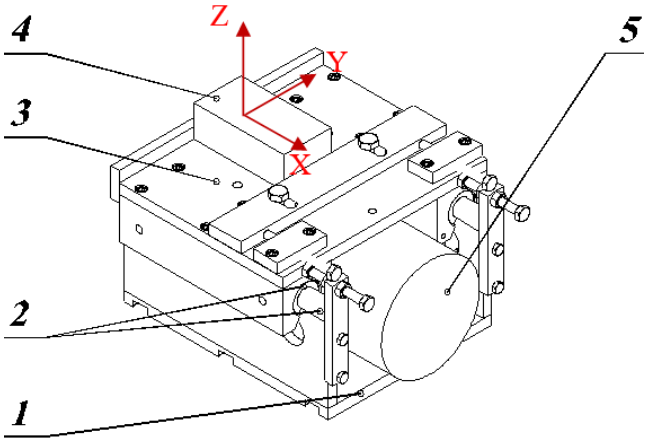


**Fig. 3.** The oscillating table

## 3. Physical model of the flat grinder

The physical model of the flat grinder, along with the grinding process without and with additional vibrations, takes into account physical phenomena occurring in the real Machine-Tool-Workpiece system: *i.e.* the gyro effect of the grinding wheel, and the regenerative self-excited vibrations, cause chatter between the workpiece and the wheel surface.

The real flat grinder structure is described with an equivalent three-dimensional physical model consisting of mass elements supported by elastic and dissipative elements. The model is presented in three orthogonal projections (XZ, YZ and XY) as shown in Fig. 4.

In the model, the elements which crucially influence the dimensional and shape accuracy of the workpiece were taken into consideration. The X-axis is collinear with feed motion of the grinder table (main tangent feed rate of $v_{ft}$); the Y-axis is along the axial vertical in-feed direction; the Z axis is in the radial in-feed direction as illustrated in Fig. 2 & 3. The physical model of the flat grinder reflects the case of up-cut grinding. The massless drive, moving with constant velocity of $v_0$, is connected to the mass $m_1$ with the spring of stiffness $k_1$ and the damper $c_1$. The mass $m_1$ stands for the table of the grinder, and it moves along the surface in the conditions of contact fluid friction described with force $F_d(\dot{x}_1)$. Spring $k_1$ and damper $c_1$ represent the stiffness and the damping of the hydraulic feed drive system, respectively.

The oscillating table with the workpiece is represented by mass $m_2$. In traditional grinding, the oscillating table is fixed motionlessly by a bolted connection. During vibratory grinding, the oscillating table with the workpiece is supported by the rolling guideways, and the superimposed harmonic oscillation of the workpiece is induced and controlled by the electrodynamic exciter. The exciter requires a preload that is applied using additional springs located between the base and the moving part of the table. The rigidity and damping of the oscillating table in the direction of the feed in up-grinding are modelled as spring $k_2$ and damper $c_2$. Mass $m_2$ can move rotationally with angular displacement of $\alpha_{2y}$. The grinding wheel unit has a mass $m_3$. The springs $k_{4x}$ and $k_{5x}$ and the dampers $c_{4x}$ and $c_{5x}$ represent the stiffness and damping of the spindle bearing system. In the machining process the grinding force components $F_n$ and $F_t$ act both on the massless point ($z_3$ coordinate) and the workpiece (mass $m_2$) [6] [7] [8] [9]. The spring $k_3$ stands for deformation stiffness of the grinding wheel in contact with the workpiece. The force $F_{w1x}$ is $x$-component of harmonic exciting force of grinding wheel unbalance.

The gyro effect occurs when the wheel is excited with the force $F_{w2}$: that is the additional excitation of the workpiece. The $x$-component of the gyro force $F_{gx}(\dot{z}_3)$ is applied to the mass $m_3$.

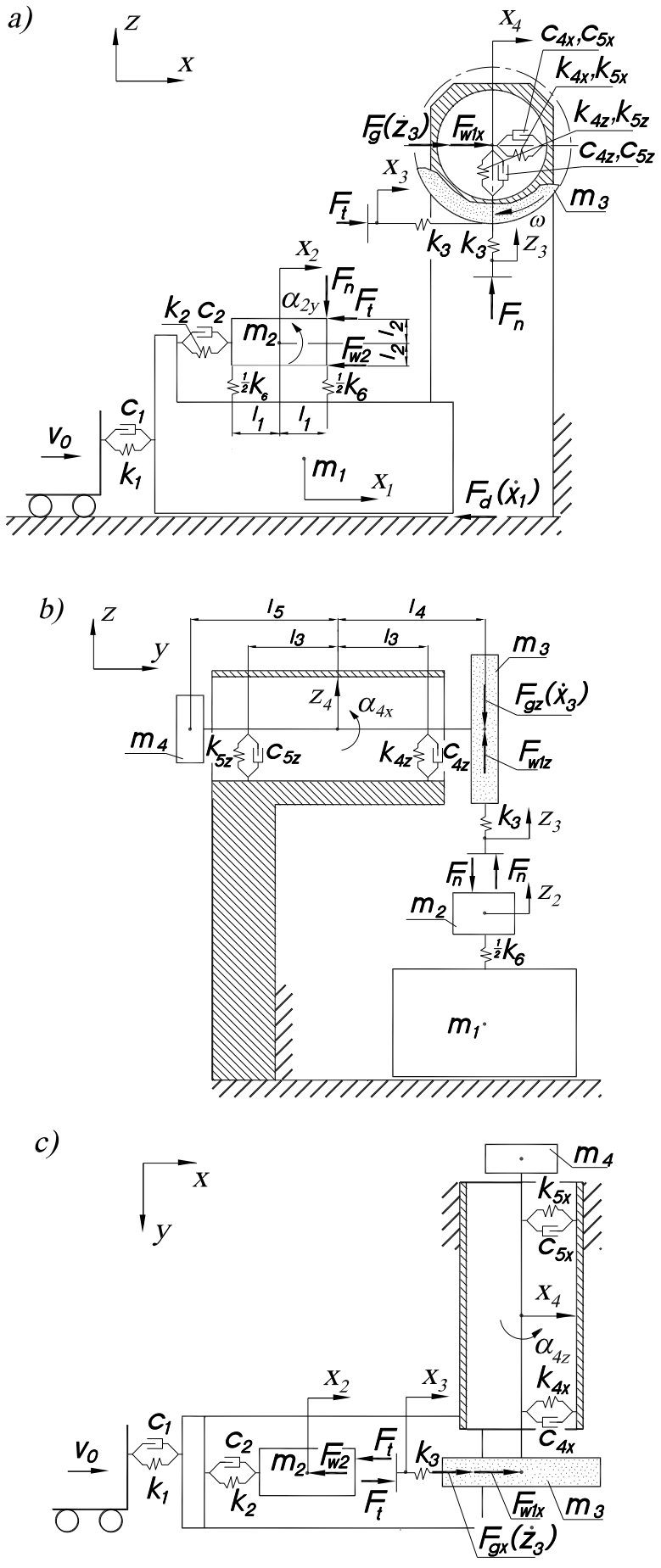


**Fig. 4.** Physical model of the flat grinder: a) front view, b) side view, c) top view

Fig. 4b represents the physical model of the Machine-Tool-Workpiece system of the flat grinder shown in YZ plane. The spindle supported with two roller bearings is modelled as rigid beam with masses at both ends and is supported with two springs $k_{4z}$, $k_{5z}$ and dampers $c_{4z}$, $c_{5z}$. The centre of gravity of the modelled spindle is in the middle of the beam. The grinding wheel has a mass $m_3$ and the spindle-driving pulley has a mass $m_4$.

The *z*-component of the harmonic excitation force $F_{w1z}$ is applied to the mass $m_3$ and is the wheel unbalance with a phase shift of $\pi/2$ reference to *x*-component of excitation force $F_{w1x}$. The *z*-component of the gyro force $F_{gz}(\dot{x}_3)$ is also applied to mass $m_3$. The oscillating table with mass $m_2$ is supported by the spring $k_6$. It is assumed that the grinder table does not move in the *z* direction. Figure 4c represents the physical model of the grinder in XY plane. The spindle in the XY and YZ planes moves around $x_4$ and $z_4$ coordinate respectively and rotates around its centre of gravity.

That physical model enables analysis of the Machine-Tool-Workpiece system dynamics by comparing the wheel behaviour in idle feed and during conventional and vibratory grinding.
Although the identification process of the model parameters takes a lot of time, the MCK approach used here (based on lumped point masses) has the advantages of being both more accurate and more detailed compared with other methods of modelling, *i.e.* hybrid modelling [10].

**4. Mathematical model**

The MCK approach is used to model the machine tool response as sets of lump masses (M), stiffness (K) and damping (C). The equations of motion of the system, as illustrated in Fig. 4, were derived as follows.

$$m_1\ddot{x}_1 + c_1(\dot{x}_1 - v_0) + c_2(\dot{x}_2 - \dot{x}_1) + k_1(x_1 - v_0 t) + k_2(x_2 - x_1) + F_d(\dot{x}_1) = 0 \quad (1)$$

$$m_2\ddot{x}_2 + c_2(\dot{x}_2 - \dot{x}_1) + k_2(x_2 - x_1) + F_t + F_{w2} = 0 \quad (2)$$

$$k_3(x_3 - x_4 + \alpha_{4z} l_4) - F_t = 0 \quad (3)$$

$$m_z\ddot{x}_4 + (c_{4x} + c_{5x})\dot{x}_4 + (c_{4x} - c_{5x})\dot{\alpha}_{4z} l_3 + (k_{4x} + k_{5x})x_4 + k_3(x_4 - x_3 + \alpha_{4z} l_4) + (k_{4x} - k_{5x})\alpha_{4z} l_3 - \{F_{w1x} + F_{gx}(\dot{z}_3)\} = 0 \quad (4)$$

$$m_2\ddot{z}_2 + k_6 z_2 + F_n = 0 \quad (5)$$

$$k_3(z_3 - z_4 + \alpha_{4x} l_4) - F_n = 0 \quad (6)$$

$$m_z\ddot{z}_4 + (c_{4z} + c_{5z})\dot{z}_4 + (c_{4z} - c_{5z})\dot{\alpha}_{4x} l_3 + (k_{4z} + k_{5z})z_4 + k_3(z_4 - z_3 + \alpha_{4x} l_4) + (k_{4z} - k_{5z})\alpha_{4x} l_3 - \{F_{w1z} + F_{gz}(\dot{x}_3)\} = 0 \quad (7)$$

$$B_{2y}\ddot{\alpha}_{2y} + k_6\alpha_{2y}l_1^2 + F_n l_1 + (F_{w2} - F_t)l_2 = 0 \tag{8}$$

$$B_z\ddot{\alpha}_{4z} + (c_{4x} + c_{5x})\dot{\alpha}_{4z}l_3^2 + (c_{4x} - c_{5x})\dot{x}_4 l_3 + (k_{4x} + k_{5x})\alpha_{4z}l_3^2 + k_3(\alpha_{4z}l_4^2 + x_4 - x_3) + (k_{4x} - k_{5x})x_4 l_3 - \{F_{w1x} + F_{gx}(\dot{z}_3)\}l_4 = 0 \tag{9}$$

$$B_z\ddot{\alpha}_{4x} + (c_{4z} + c_{5z})\dot{\alpha}_{4x}l_3^2 + (c_{4z} - c_{5z})\dot{z}_4 l_3 + (k_{4z} + k_{5z})\alpha_{4x}l_3^2 + k_3(\alpha_{4x}l_4^2 + z_4 - z_3) + (k_{4z} - k_{5z})z_4 l_3 - \{F_{w1z} - F_{gz}(\dot{z}_3)\}l_4 = 0 \tag{10}$$

The force of unbalance $F_{w1}$ applied to mass $m_3$ is defined as follows

$$F_{w1} = A_1 \sin \omega_0 t = m_d r \omega_0^{\,2} \sin \omega_0 t\,, \tag{11}$$

The model and the equations of motion are used to study the dynamic response of the machine tool system and the process during conventional and vibratory grinding. In conventional grinding the excitation force $F_{w2} = 0$, whereas in vibratory grinding this force is the harmonic excitation provided by the oscillating table:

$$F_{w2} = A_2 \sin(2\pi f t), \tag{12}$$

In conventional grinding, the oscillating table is fixed motionless, thus, the stiffness $k_2$ and viscous damping $c_2$ are different in vibratory grinding.

The normal grinding force $F_n$ (eq.5 and eq.6) were defined using the approach formulated for typical grinding process [12] and further adapted to account for the variations in speed of the table (induced vibrations) and regenerative effect of wheel and workpiece surfaces (wheel/workpiece chatter). The resulting expression of the normal grinding force $F_n$ is as follows:

$$F_n = b_D K (C_{St1})^{\gamma} \left( \frac{v_{ft} + v_{w2}(t)}{v_s} \right)^{2\varepsilon - 1} [a_n + a_{ew}(t) + a_{es}(t)]^{\varepsilon} (d_s)^{1-\varepsilon}\,, \tag{13}$$

The regenerative effect plays a crucial role in grinding. The sources of the regenerative vibration can be found in either the shape modification of a non-uniformly worn grinding wheel and/or in variations in the shape of the workpiece [13]. The explanation of this phenomenon consists in the assumption that the workpiece profile $a_{ew}(t)$ can be calculated by subtracting the previously shaped profile $a_w(t-\tau_p)$ from the actual profile $a_w(t)$ (eq. 14). The non-uniformities of the grinding wheel shape are taken into account (eq. 15) in the same way. The regeneration effect on the workpiece and grinding wheel is expressed in the grinding force expression (eq. 13) in the form of time delays $\tau_p$ and $\tau_s$ as shown in eq. 14-15:

$$a_{ew}(t) = a_w(t) - a_w(t-\tau_p), \tag{14}$$

$$a_{es}(t) = a_s(t) - a_s(t-\tau_s), \tag{15}$$

The tangential grinding force is expressed as $F_t=\mu F_n$, [12] (16)

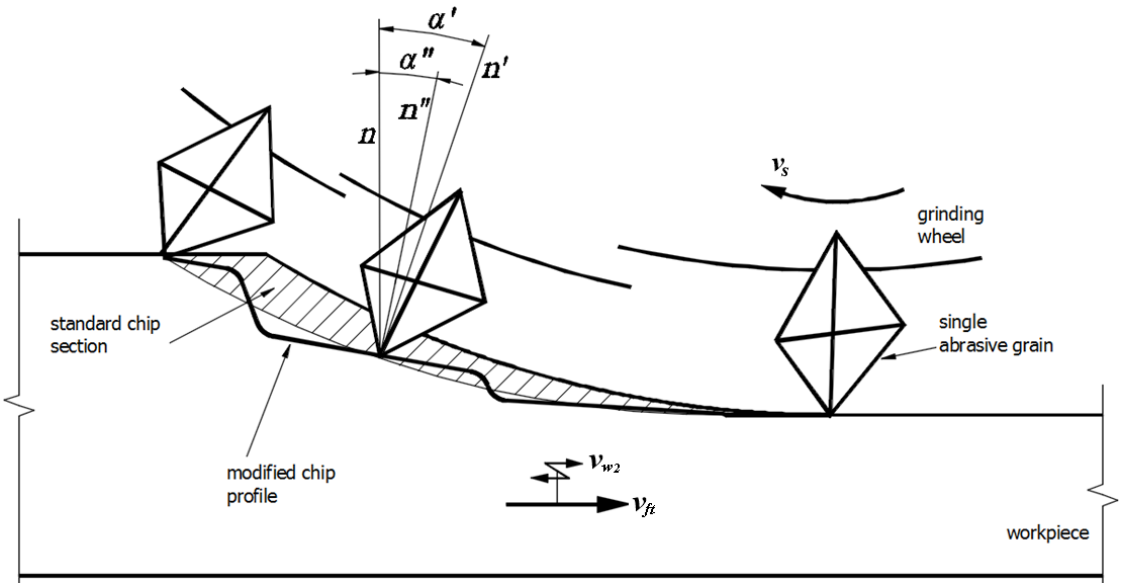


**Fig. 5:** Sketch of the kinematics of single grain in up-grinding with superimposed vibrations

In the vibratory grinding process the contact length of the single grain with the workpiece varies in time. The sketch in Fig. 5 illustrates the kinematics of the single cutting grain in the up-grinding process, with additional vibration of the workpiece, where the grain is rotating at wheel speed $v_s$ and the workpiece translates at tangential feed $v_{ft}$. In conventional grinding, the grain removes a chip, which is represented by the hatched section. If the constant motion $v_{ft}$ of the workpiece is superimposed with the harmonic oscillation of the tangential feed, $v_{w2}=A_2\ sin(2\pi ft)$, it results in a modulation of the chip cross-section as depicted in Fig. 5 (modified chip profile).

One of the main features of the dynamics of the grinding process is the elastic deformation of the grinding wheel. This is of a great importance considering the dynamic stability of the process. The contact stiffness is defined as a ratio of the normal compressive force $F_n$ and elastic deformation $\delta$ of the wheel in the contact zone. In the theoretical studies of the elastic contact deformation $\delta$ the Hertz contact model is usually applied [14]:

$$\delta = F_n^{\rho}, \tag{17}$$

here the exponent $\rho<1$,

The contact stiffness $k_3$ is nonlinear in principle, and can be defined as follows:

$$k_3 = \frac{dF_n}{d\delta} \tag{18}$$

Considering equations (13) and (17), the contact stiffness can be expressed as a function of selected grinding parameters. For instance, the increase of ratio $v_s/v_w$ and/or depth of cut results in an

increase of contact stiffness in grinding and this was also investigated experimentally [4] [13] [15]. It was shown that in these that higher-grade wheels (hard wheels), the hardness led to a significant increase in contact stiffness. In the work presented in this paper, the contact stiffness $k_3$ was determined experimentally. The whole process of the contact stiffness determination is described in [9].

In the mathematical model (eqs.1-10), the gyroscopic effect in both conventional and vibratory grinding is expressed by forces $F_{gz}(\dot{x}_3)$ and $F_{gx}(\dot{z}_3)$, as illustrated in Fig. 6.

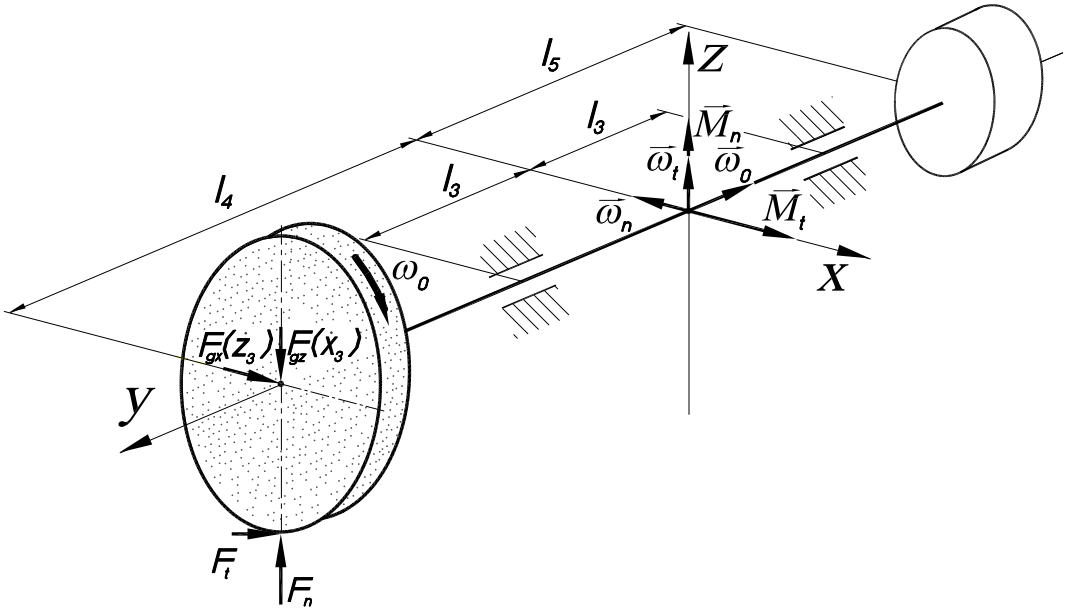


**Fig. 6:** Gyro-effect of the grinding wheel spindle unit $\omega_0$

The origin of the coordinate system is in the centre of gravity of the investigated system. The grinding wheel rotational speed is $\vec{\varpi}_0$. The normal ($F_n$) and tangent ($F_t$) grinding force results in precession motions of rotational speed $\vec{\varpi}_n$ and $\vec{\varpi}_t$ respectively; this gyroscopic phenomenon engenders torques $\vec{M}_n$ and $\vec{M}_t$. These gyro-torques are determined as follows:

$$M_n = J\omega_0\omega_n\,, \tag{19}$$

$$M_t = J\omega_0\omega_t\,, \tag{20}$$

The gyroscopic forces affecting the grinding wheel in surface grinding are determined as follows:

$$F_{gx}(\dot{z}_3) = \frac{M_n}{l_4} = \frac{J\omega_0\omega_n}{l_4} = \frac{J\omega_0}{l_4^{\,2}}\,\dot{z}_3\,, \tag{21}$$

$$F_{gz}(\dot{x}_3) = \frac{M_t}{l_4} = \frac{J\omega_0\omega_t}{l_4} = \frac{J\omega_0}{l_4^{\,2}}\,\dot{x}_3\,, \tag{22}$$

It is observed that the equations of motion (eqs.1-22) describing process behaviour in conventional and vibratory grinding are highly non-linear. Therefore, the solutions for these equations were obtained using numerical methods implemented in Matlab-Simulink. Here Dortmand-Prince's method that is based on Runge-Kutta integrator was used with a time step of 0.0001 and stable wheel speed.

## 5. Simulation

In order to assess the adequateness of the physical model and its compatibility with the real system behaviour, an amplitude- frequency (AF) characteristics of the grinding wheel spindle was investigated in *x* and *z* direction, and the results are presented in Fig.7 and 8 respectively. Here, a sinusoidal excitation force at frequencies ranging from 1 to 500 Hz was applied to the system. The simulation was undertaken for an idle non-rotating spindle excited with a harmonic force at constant amplitude.

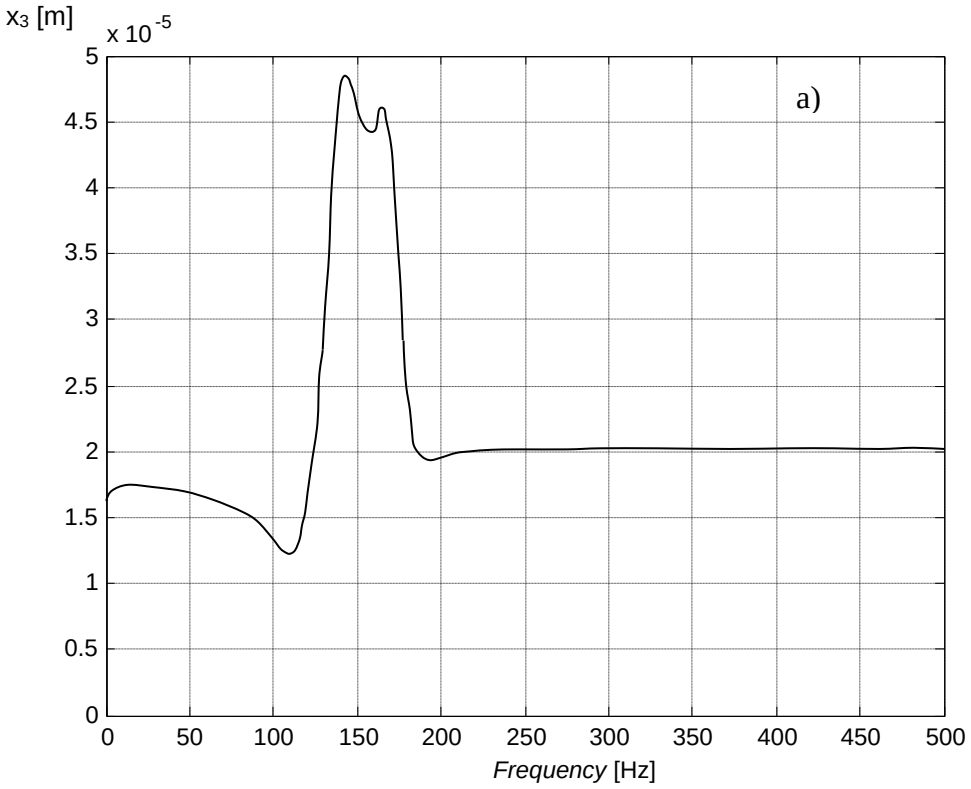


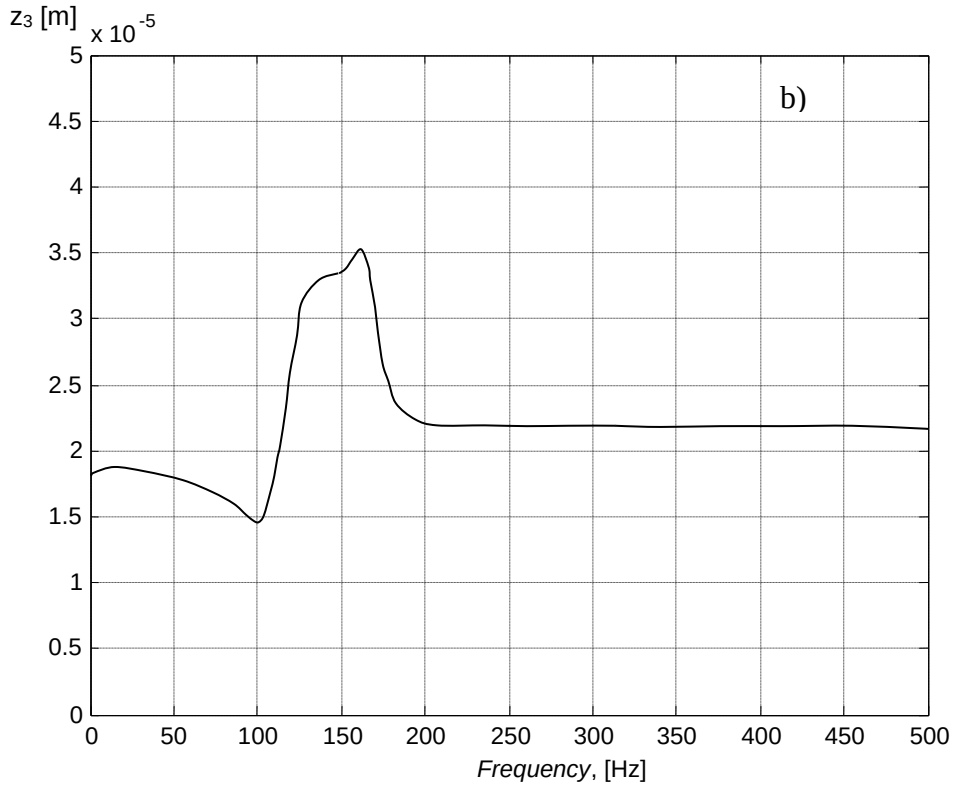


**Fig. 7.** Wheel spindle Amplitude-frequency response: a) x direction; b) *z* direction

Figure 7 illustrates the response of the contact point $x_3$ between the grinding wheel and the workpiece, showing a resonance amplitude at a frequency of 140 Hz in the *X* direction and of 160 Hz in the *X* direction.

The investigation into the dynamic response of system was performed in two stages, in conventional regime and in vibratory mode using appropriate phase shift of the eccentricity of the grinding wheel (forces $F_{w1x}$ and $F_{w1z}$). In the first stage, the dynamic response of the normal and tangential grinding forces $F_n$ and $F_t$ in conventional grinding was investigated. Here, the regenerative effects of the workpiece and grinding wheel were taken into account, along with the gyroscopic forces $F_g(\dot{z}_3)$ and $F_g(\dot{x}_3)$, which are induced by the appearance of the grinding force at the moment of contact of the wheel and the workpiece.

**Table 1**: Variables and process parameters

| Parameter | Values | Parameter | Values, m | Parameter | Values |
|---|---|---|---|---|---|
| $m_1$, kg | 100 | $l_1$ | $105\ 10^{-3}$ | $v_0$, m/min | 1, 5, **10**, 15, 20 |
| $m_2$, kg | 7.5 | $l_2$ | $55\cdot10^{-3}$ | $a_n$, mm | 0.001, **0.005**; 0.01, 0.02; 0.03 |
| $m_z$ , kg | 6 | $l_3$ | $100\cdot10^{-3}$ | $d_s$, mm | 180; 190; **200** |
| $B_{2y}$ , kgm$^2$ | 0.0345 | $l_4$ | $190\cdot10^{-3}$ | $A_0$, μm | 1; 5; **10**; 20 |
| $B_z$ , kgm$^2$ | 0.152 | $l_5$ | $160\cdot10^{-3}$ | $A_{vib}$, μm | 9 |
| $k_1$ , N/m | $392.5\cdot10^6$ | | | $f_{vib}$, Hz | **140** |
| $c_1$ , Ns/m | 2626 | | | | |
| $k_2$ , N/m | $4.86\cdot10^6$ | | | | |
| $c_2$ , Ns/m | 631.6 | | | | |
| $k^*_2$ , N/m | $1.44\cdot10^6$ | | | | |
| $c^*_2$ , Ns/m | 541.7 | | | | |
| $k_3$ , N/m | $6.6\cdot10^6$ | | | | |
| $k_{4x}$=$k_{5x}$, N/m | $8.72\cdot10^6$ | | | | |
| $c_{4x}$=$c_{4x}$, Ns/m | 485.13 | | | | |
| $k_{4z}$ = $k_{5z}$, N/m | $7.2\cdot10^6$ | | | | |
| $c_{4z}$ = $c_{5z}$, Ns/m | 920.4 | | | | |
| $k_6$ , N/m | $49.1\cdot10^6$ | | | | |

In the second phase of the modelling, the vibration assisted grinding was investigated by allowing the vibratory table to oscillate, consequently, adding stiffness $k_2$ and damping $c_2$ and activating stiffness $k^*_2$ and damping $c^*_2$ of the vibrating table. Here, the vibration of the workpiece is driven by the force $F_{w2}$ excited in the tangential (X) direction. The list of parameters used in this study is given in table 1.

The study showed that a reduction of the vibration of the wheel relative to the workpiece in *z* direction was achieved when the introduced vibration had an amplitude of 9 μm at 140 Hz. The gyro phenomenon had no significant effect on the dynamics of the process modelled here for surface grinding. The results of the simulation presented here are for the following parameters: $A_0$ = 10 μm, $v_0$ = 10 m/min, $a_n$ = 0.005 mm with a wheel diameter $d_s$ = 200 mm. As in real grinding the simulation had an actual grinding phase at full depth of cut, for a duration of 0.15s, and a spark-out of 0.15s. To reduce computing time and power requirements, a short simulation time was set for the grinding and spark-out phases.

In grinding, the geometric accuracy and roughness of the machined surface is highly affected by the vibrations of the wheel relative to the workpiece in the *Z* direction. Therefore, an investigation was carried out in z-direction to quantify this effect using the model developed.

Figures 9 and 10 show the time dependent response of the grinding wheel and the workpiece in *z* direction respectively for conventional and vibratory grinding. For conventional grinding, Fig. 9a and Fig.10 show a gradual increase in wheel vibration amplitude due to the regenerative effect. In general, the wheel deflects slightly up due to the normal grinding force acting upwards. Additionally, in the first and second run (up to t=0.30s) the amplitude of the wheel displacement stays comparatively low. That is the result of the damping property of the grinding process. Authors [16] proved that during grinding, the higher depth of cut, the higher damping of the grinding process is observed; however, because of the dynamic instability of the system, the amplitude during the second and further spark-out passes keeps growing. A beating effect is also observed in Fig.9a and Fig.10, however fig.9b shows that for vibratory grinding a stable amplitude of the grinding is achieved, due to the induced relief (reduction in forces) on the grinding wheel.

Similarly, Fig.11b in vibratory grinding after t=0.30s the position of the wheel stabilised with a much lower amplitude than that of conventional grinding (Fig.11a). A significant release of stress is observed with mean value close to zero. The most important development is the fact that the amplitude of the wheel in *z* direction in the second and further passes stays at the same level and does not grow. This proves that the superimposed vibration on the workpiece in the feed direction of the table counteracts the instability of the process. This is explained by the "periodical relief" – meaning that the applied vibration periodically reduces the force applied to the tool, and this intermittent relief supresses the build-up phenomenon of the self-excitation, regenerative and beating process that is seen in Figures. 9-11. Stone [17] pointed out the theoretical possibility of enhancing stability, by minimizing the angle of natural frequency mode direction and the direction of depth of cut. In his work, Stone showed that minimizing the angle leads to an effective increase of structural damping in grinding process and decrease of magnitude of regenerative chatter.

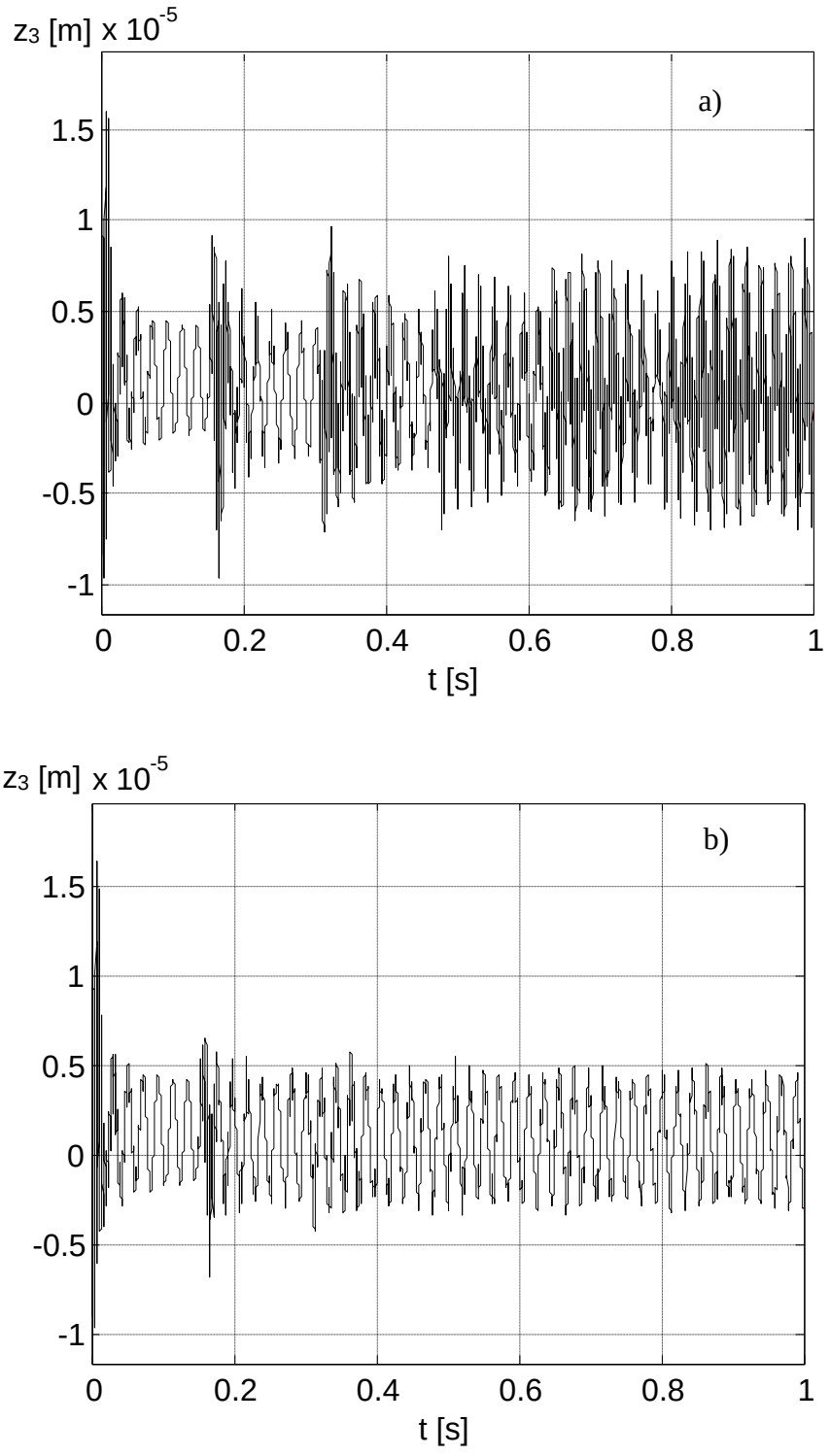


**Fig. 9.** Time dependent of grinding wheel position in *z* direction:
a) conventional grinding; b) vibratory grinding

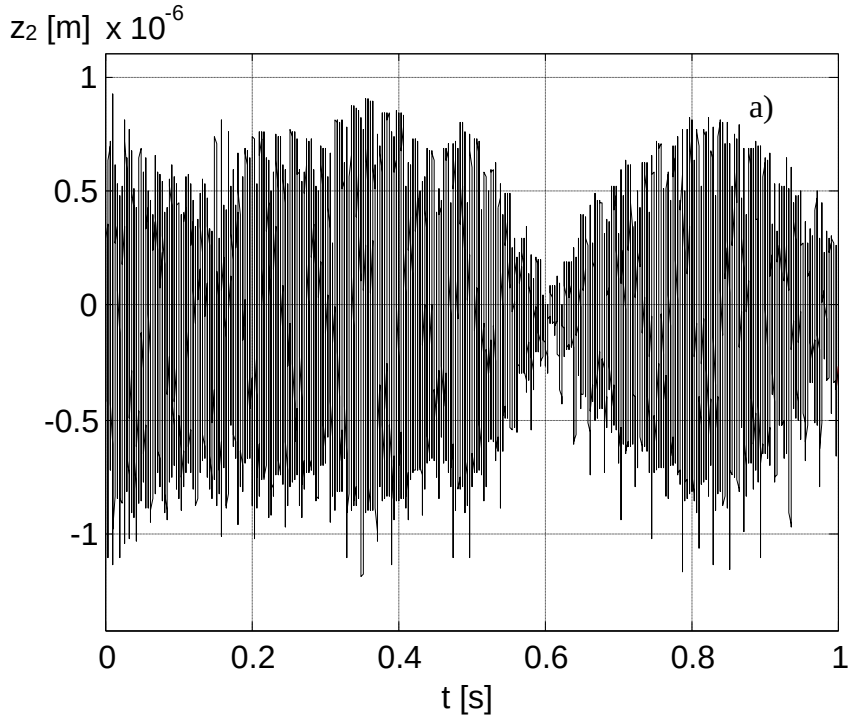


**Fig. 10.** Time dependent of the workpiece position in *z* direction for conventional grinding.

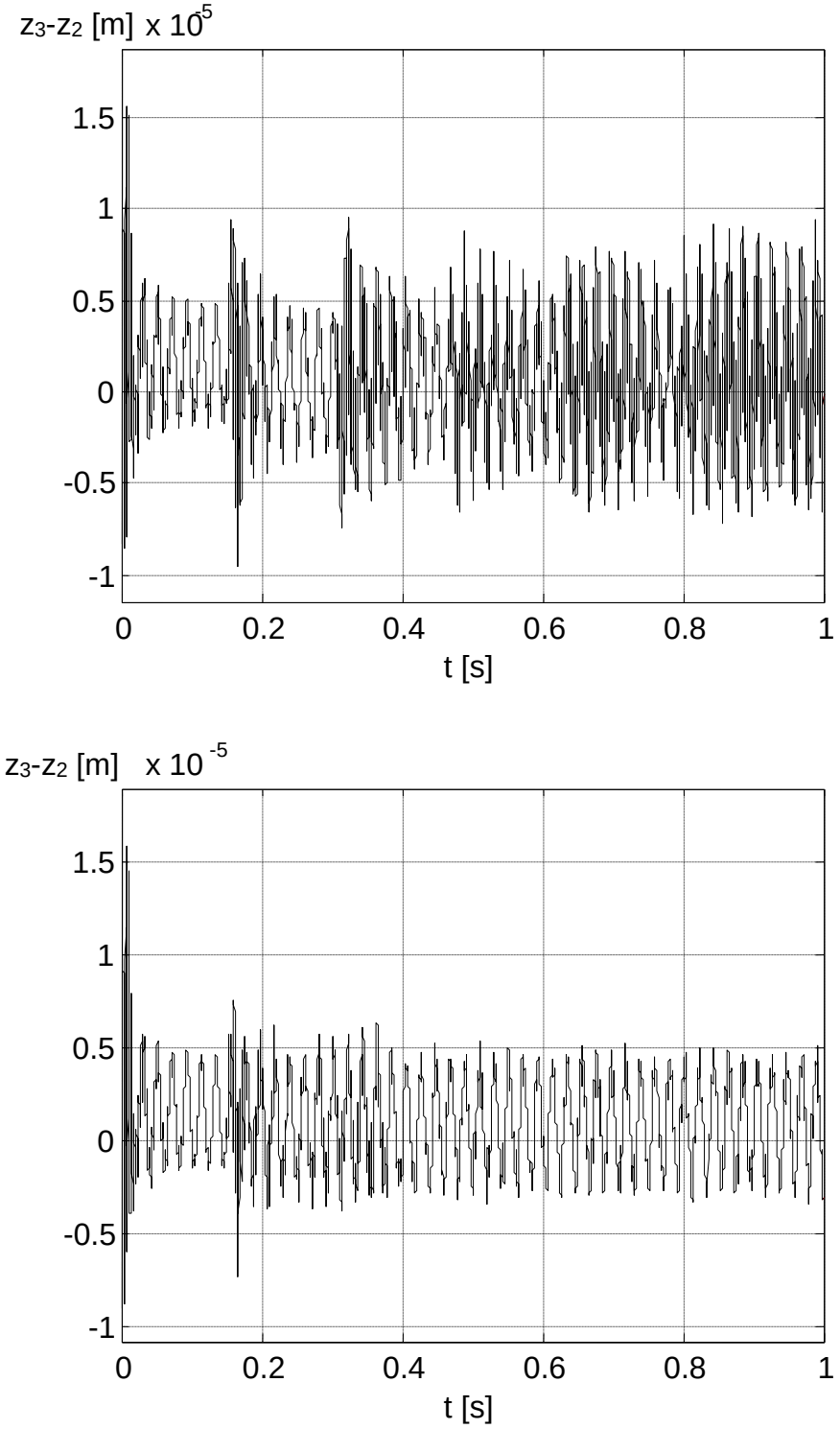


**Fig. 11.** Time dependent of the relative position of the grinding wheel and the workpiece in *z* direction for: a) conventional grinding and b) vibratory grinding

Fig. 5 illustrates that the standard and modified chip profiles significantly differ in an average angle (α' and α") of the profile line (*n'* for conventional and *n"* for vibratory grinding profile) in relation to the main natural frequency mode direction (vertical line *n*). Superimposing vibration to the workpiece movement leads to a reduction of this angle in terms of single grain path; thus, increasing stability and damping on the one hand. On the other hand, the improved performance of the system is conditioned by the overall dynamic relief the load applied to the cutting grits due to the superimposed vibratory process. This relief is the ratio of the average oscillatory cutting to magnitude of cutting in conventional grinding [22-23]. This ratio is always *less than one* and lower it is the better is the performance. In general, the relief induced by vibratory processes is expressed as $\beta = \frac{Average\ vibratory\ process\ force}{Force\ required\ in\ conventional\ process}$

The phenomenon of achieving lower grinding force when adding oscillation to one of the kinematic motion of grinding was observed by Tsiakoumis and Batako [18]. Drew, *et al*, [21], in their experimental work, found that in conventional grinding, the specific chip formation energy was about twice the energy required for vibratory grinding with oscillations of the workpiece speed. This improved performance of vibratory grinding is explained by an effective removal of the built-up from the cutting edges, the removal of the ground material from grains spaces preventing wheel clogging, which promote the exposure of clean cutting edges of the grits.

## 6. Experimental work and results

An experimental work was undertaken with a range of grinding process parameters. Here soft and hardened steel were ground with varying depths of cut and frequencies. The feed rate and the wheel were kept constant. The grinding process was in dry conditions using two types of grinding wheels (St-Gobain Altos Porous wheel with needle-like grain and a medium grade Wheel - 454A601L7GV3). Two types of workpiece materials were used, namely, a mild Steel (BS970 080440), and a hardened M2 (62HRC) tool steel (BS BM2) and EN31 (64HRC). The wheel Speed was constant at 35 m/s and the vibration frequency was 100, 140 200, 250 300 Hz at a vibration amplitude of 15 μm.

The following results present the process performance for both conventional and superimposed vibrational grinding using the 454A601L7GV3 wheel. The wheel was dressed and conditioned for each grinding trial.

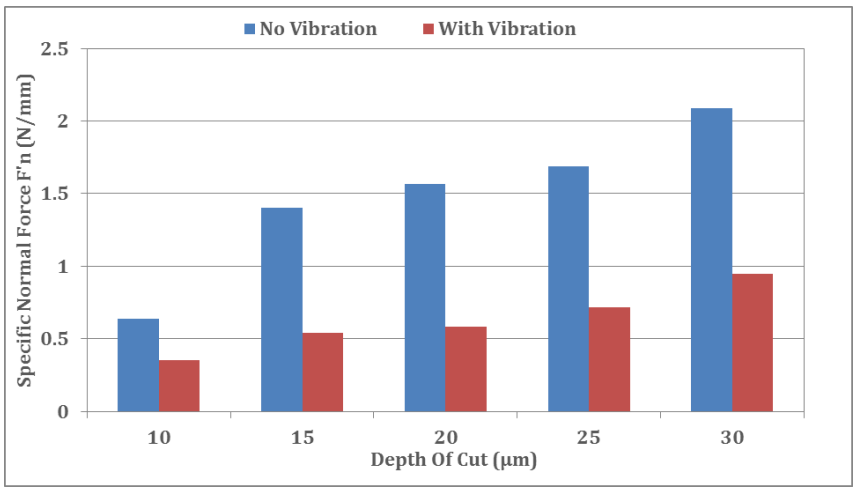


Fig. 12: Normal grinding force for Hardened steel 64HRC.

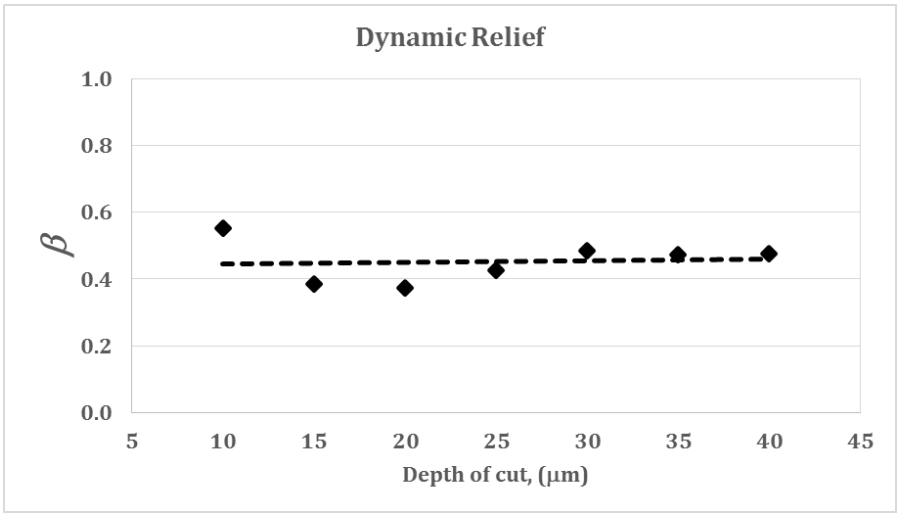


Fig. 13: Dynamic relief induced by vibratory process.

Fig.12 illustrates the specific normal cutting force for grinding hardened steel in conventional and vibratory mode. It is observed here that the vibratory process outperformed the conventional process. Fig.13 shows the corresponding dynamic relief, which directly supports the findings of Drew [21] who stated a two-fold reduction in specific energy requirement in oscillatory grinding. It is seen here, that over the entire range of depths of cuts, the vibratory process secured an average dynamic relief around 0.5

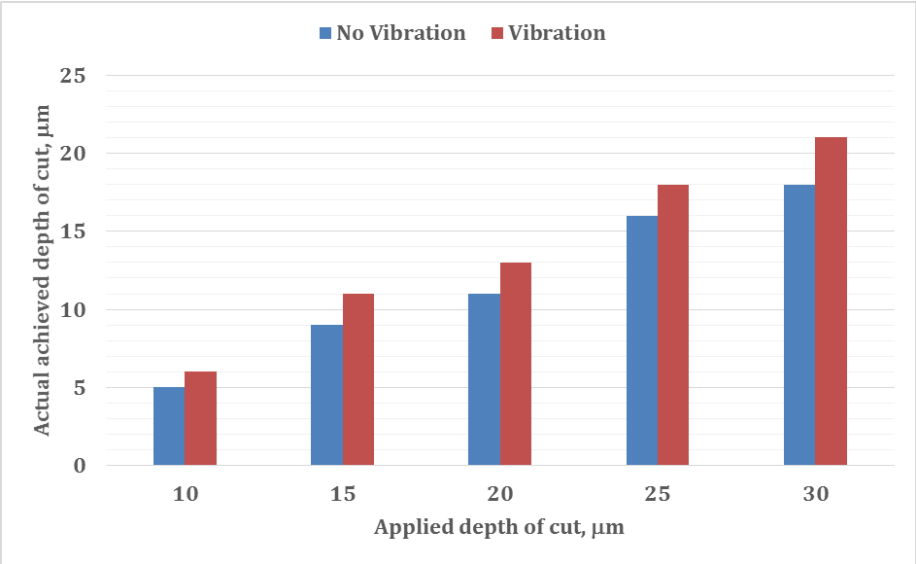


Fig.14: Comparative actual achieved depth of cut

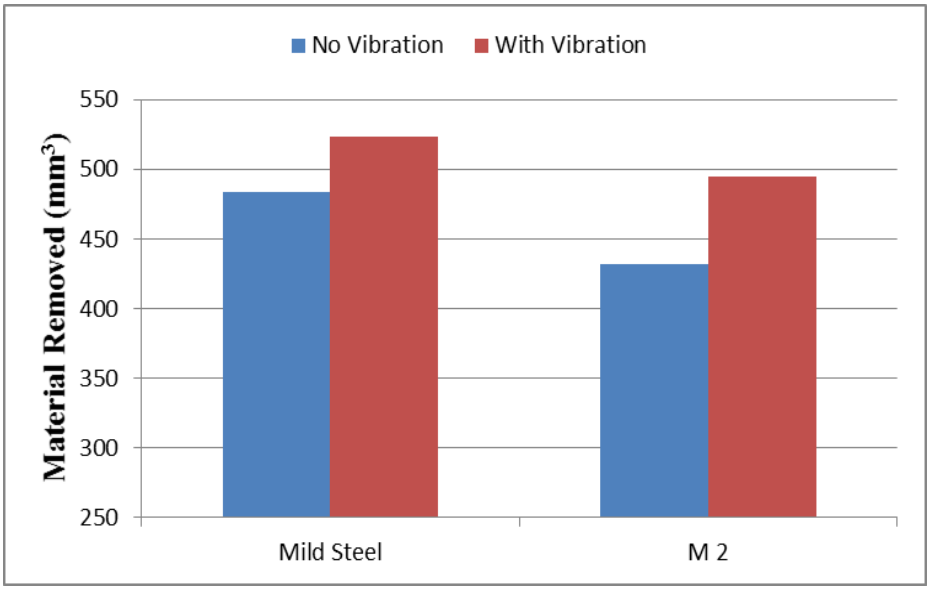


Fig.15: Material Removed for 454A 601L7GV3 grinding wheel.

Fig.14 and 15 depict exceptional performance or even a paradox because referring to Fig.12 where vibration led to lower cutting forces, one would expect low material removed. Conversely, Fig.14 shows that the application of vibration provides a better cutting achieving higher real depth of cuts compared to conventional continuous cutting process. It was observed that at frequencies over 200Hz, the superimposed vibration allowed removing exactly the applied depth of cut. This was recorded for depth of cuts above 20 µm, this is reflected towards the end of the dynamic relief graph where 30-35-40 µm gave the same ratio $\beta$. It is worth mentioning that the grinding machine used in this study is old and has low stiffness.

Equally, Fig.15 portrays a comparative performance of the process in terms of material removal, where, the vibration secured a higher amount of material removed. The mild soft steel quickly clogged the grinding wheel in conventional grinding but the wheel stayed clean and sharp in vibratory process. The application of vibration has a net advantage over conventional grinding in both soft and hardened steels.

To study the wheel life, successive 10 μm depths of cut were applied to the wheel I reciprocated mode and a set amount of material was removed from the workpiece. In this test, the total depth of cut applied to the wheel was 1 mm, and after grinding, the actual total depth of cut was measured and the volume of material removed was calculated. A razor blade was used to imprint the wear profile of the wheel surface, subsequently, the blade was measured using Tailor-Hobson profiler, thus allowing the wheel surface wear to be quantified.

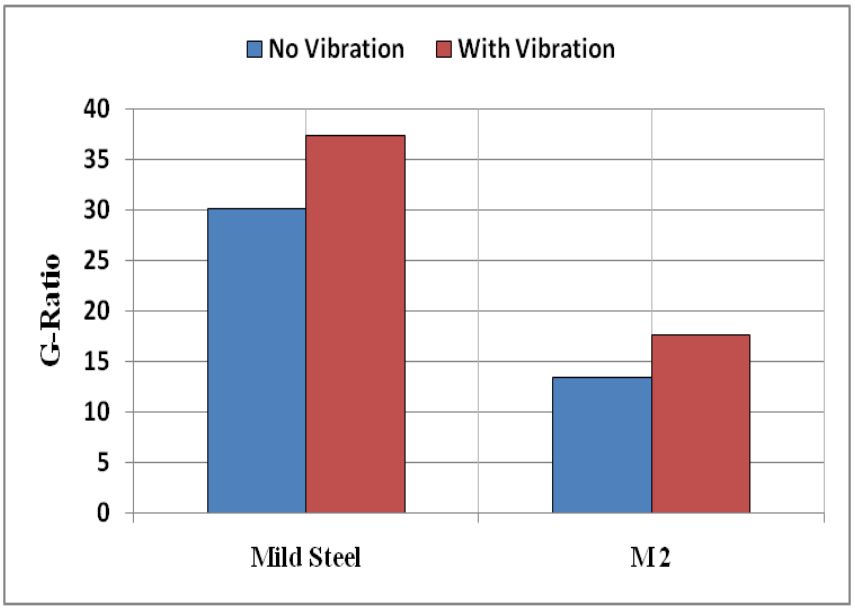


Fig.16: Wheel performance - G-Ratio

Fig.16 shows the grinding wheel life in terms of G-ratio for conventional and vibration-assisted grinding. Regardless of its higher volume of material removed, vibro-grinding secured a better wheel life. The result of wheel life in grinding mild steel support the statement made above that added vibration kept the wheel clean and sharp, allowing it to cut better without wearing too much.

Owing to the fact that the experiments were done in dry condition, which is harsh for any grinding process, it is speculated that the superimposed vibration brings a net benefit in absolute terms, including flood coolant supply and minimum quantity lubrication.

## Conclusions

A mathematical model of a surface grinding machine was presented as a first step in the modelling of vibratory grinding. Subsequently a cutting force model was derived and an oscillatory motion was added to the feed motion. The model took into account various aspects of grinding including the gyroscopic effects.

The numerical values for the parameters used in the model were experimentally derived for a real surface grinding machine tool, this allowed the results to be realistic.

The results of the modelling showed that the regenerative and self-excited vibration lead to beating phenomenon in the grinding process which affect the process performance, e.g. surface waviness.

The modelling also showed that the introduction of vibration into the feed motion counteracted the detrimental self-excited and regenerative vibration, which led to an improved system performance.

The experimental work showed that the superimposed vibration to the grinding process secured a superior performance of the machining in terms of cutting forces, material removed and actual depth of cuts. The application of vibration provided low cutting forces, with high removal rates along with an extended wheel life.

A "dynamic relief" coefficient $\beta$ was derived to characterise the performance of vibro-grinding relative to conventional grinding. It was shown that the lower the coefficient of dynamic relief $\beta$ the better the performance of the induced vibration. Here the dynamic relief was on average 0.5 which means that the vibratory process required only half of the energy used for conventional grinding to achieve the same volume of material removal.

It is therefore speculated that a well-designed and controlled low frequency vibration has a greater potential than current conventional processes for the machining of a wide variety of material types, and without the need of high frequencies as used in ultrasonic grinding.

References


[1] Kruszynski B.; Midera S., Kaczmarek J.: *Forces in generating gear grinding-theoretical and experimental approach*, CIRP Annals-Manufacturing Technology, vol. 47/1/1998, pp. 287-290.

[2] Marchelek K.: *Dynamika obrabiarek (Dynamisc in Machine Tools* – in Polish*).* Wyd. II, WNT, Warszawa 1988.

[3] Wrotny L. T. *Fundamentals of the machine tools constructions – (in Polish).* WNT, Warszawa 1973.

[4] Inasaki I.: *Grinding of Hard and Brittle Materials*. Annals of the CIRP, vol. 36/2/1987, pp. 463-471.

[5] Oczos K. E.: *Ksztaltowanie ceramicznych materiałow technicznych (Shaping the ceramic materials* – in Polish*).* Oficyna Wydawnicza Politechniki Rzeszowskiej, Rzeszow 1996.

[6] Orynski F., Bechcinski G.: *Badania symulacyjne drgan sciernicy szlifierki do plaszczyzn z wrzecionem ułozyskowanym hydrostatycznie (Simulation research of vibrations of the flat grinder with hydrostatic bearing of the spindle* – in Polish). V Sci-Tech Conference: Gas and Hydrostatic Bearings, Lodz 2000, pp. 97-107.

[7] Orynski F., Bechcinski G.: *Badania symulacyjne drgan sciernicy szlifierki do plaszczyzn z wrzecionem ułozyskowanym tocznie (Simulation research of vibrations of the flat grinder with roller bearing of the spindle* – in Polish). XXIV Conference - Scientific School of Abrassive Machining, Krakow - Lopuszna 2001, pp. 333-340.

[8] Orynski F., Pawlowski W.: *The mathematical description of dynamics of the cylindrical grinder*. International Journal of Machine Tools and Manufacture, No 42/7, 2002, pp.773-780.

[9] Orynski F., Pawlowski W.: *Simulation and Experimental Research of the Grinder's Wheelhead Dynamics.* International Journal of Vibration and Control, vol. 10/6/2004, pp. 915-930.

[10] Pawlowski W.: *Dynamic Model of Oscillation-Assisted Cylindrical Plunge Grinding with Chatter*. Journal of Manufacturing Science and Engineering, 135(5):051010-051010-6, doi:10.1115/1.4024819.

[11] Bechcinski G.: *Aktywne oddziaływanie poprzez drgania na zmniejszenie falistosci szlifowanych powierzchni plaskich (Active interacting by means of vibrations in order to achieve lower waviness of ground flat surfaces* – in Polish). PhD Thesis, Politechnika Lodzka, 2006.

[12] Oczos K. E., Porzycki J.: *Szlifowanie - podstawy i technika (Grinding – Fundamentals and Technique* -in Polish). WNT, Warszawa 1986.

[13] Plaska S.: *Influence of dynamic parameters of grinding process on shape errors of the machined surface – (in Polish);* PhD Thesis, Politechnika Lodzka, 1979.

[14] Inasaki I., Karpuschewski B., Lee H.-S.: *Grinding Chatter – Origin and Suppression.* Annals of the CIRP, vol. 50/2/2001, pp. 1-20.

[15] Inasaki I.: *Selbsterregte Ratterschwingungen beim Schleife, Methoden zu ihrer Unterdrückung.* Werkstatt und Betrieb, 110/8/1977: 521-524.

[16] Orynski F., Pawlowski W.: *The influence of grinding process on forced vibration damping in headstock of grinding wheel of cylindrical grinder.* International Journal of Machine Tools and Manufacture, No 39, 1999, pp.229-235.

[17] Stone B.: *Chatter in Machine Tools.* DOI: 10.1007/978-3-319-05236-6, Springer 2014.

[18] Tsiakoumis V., Batako A.: *Vibration-Assisted Grinding of Mild and Hardened Steel: A Novel Design Vibrating Jig and Process Performance.* ASME 2012 11th Biennial Conference on Engineering Systems Design and Analysis.

[19] Batako Andre D.L. and Tsiakoumis Vaios, (2014), An Experimental Investigation into Resonance Dry Grinding of Hardened Steel and Nickel Alloys with element of MQL; Int J Adv Manuf Technol (in press); DOI: 10.1007/s00170-014-6380-8

[20] Tsiakoumis V. & Batako A. D, (2012), Vibration assisted surface grinding of mild and hardened steel: Performance of a novel vibrating jig design, *Proceedings of the 37th International MATADOR Conference 2012*, Manchester, July 2012, 185-188

[21] Drew S.J., Mannan M.A., Ong K.J., Stone B.J.: *The measurement of forces in grinding in the presence of vibration*. International Journal of Machine Tools and Manufacture, 41(4), 2001, pp. 509-520.

[22] Astashev V.K., Babitsky V.I., Kozlov M.Z., (2000), Dynamic control of machines, Springer-Verlag, Berlin.

[23] Batako A.D.L. (2003), A self-exciting system for percussive-rotary drilling, PhD thesis, Loughborough University, UK.